GeoStorage

Vol. 2, No. 1, p. 61-77, 2026

Research article

Study on the Inhibitory Effect and Patterns of Backfilling Salt Caverns with Waste Alkali Slag on Surface Subsidence in Mining Areas

Xiangsheng Chen[1,2]*, Feng Lin[1], Mingnan Xu[2]*, Yalong Jiang[1], Ahu Zhao[2], Xilin Shi[2], Yinping Li[2]

[1] *State Key Laboratory of Safety and Resilience of Civil Engineering in Mountain Area, East China Jiaotong University, Nanchang 330013, China*

[2] *State Key Laboratory of Geomechanics and Geotechnical Engineering Safety, Institute of Rock and Soil Mechanics, Chinese Academy of Sciences, Wuhan 430071, China*

Keywords:

Rock salt
surface subsidence control and prediction
backfill alkali slag
long-term stability analysis
solution mining

Cited as:

Chen XS, Lin F, Xu MN, et al. 2026. Study on the Inhibitory Effect and Patterns of Backfilling Salt Caverns with Waste Alkali Slag on Surface Subsidence in Mining Areas. *GeoStorage*, 2(1), 61-77.
https://doi.org/10.46690/gs.2026.01.05

Abstract:

The excellent physical and mechanical properties of rock salt have led to the rapid development of salt mine exploitation, giving rise to various types of salt cavern energy storage facilities. However, the geological hazards and environmental issues associated with this development cannot be ignored. This study focuses on 16 pairs of brine extraction caverns in a real salt mine in China. Based on the engineering geological conditions of the mine, existing drilling and geophysical data, salt mining activities, sonar cavern measurements and other relevant data, a three-dimensional dynamic analysis model for subsidence in salt mining areas was proposed. By fully considering the influence of dynamic backfilling with alkali slag on surface subsidence, subsidence predictions for the next 50 years and long-term stability evaluations were conducted, clarifying the subsidence deformation patterns and the development trend of the subsidence center. These results are generally consistent with the mining plan of the salt mine. The study shows that the proposed model can accurately reflect the inhibitive effect of backfill alkali slag on salt cavern creep shrinkage and reproduce the subsidence patterns of the strata and surrounding buildings (with an error margin within 15%), demonstrating good applicability and accuracy. The overall subsidence in the target mine area presents a large-scale, slow, uniform, and gradually converging trend over time. The subsidence difference and tilt rate also meet the requirements of standards in China, ensuring long-term stability. The findings of this study provide analytical insights for surface subsidence prediction and ground stability analysis in salt mining areas, offering valuable references and guidance for subsidence control in similar engineering projects.

1 Introduction

Ground surface subsidence is an inevitable and significant issue in mineral extraction and underground engineering construction (Bell et al., 2000; Li et al., 2004). Rock salt is not only a scarce mineral resource but also an excellent site for underground energy storage, with its development and utilization now entering a rapid growth phase. The cavities (salt caverns) left behind after salt mining are widely used for compressed air energy storage, natural gas storage, hydrogen storage, helium storage, and nuclear waste disposal (Chen et al., 2024; Evans et al., 2021; Liu et al., 2023; Minkley et al., 2022; Tarkowski and Uliasz-Misiak, 2022). However, the geological hazards and environmental impacts associated with these activities cannot be overlooked, particularly the safety hazards posed by abandoned salt caverns.

As shown in Fig.1, In 2010, a ground subsidence occurred at the Jiu'er Salt Mine in Jiangxi, China, with a subsidence area of approximately 3000 m^2 (Bai et al., 2024; Yao et al., 2011). The

* Corresponding author.
E-mail address: chenxs15@163.com (Chen XS); lin13659864130@163.com (Lin F); mnxu@whrsm.ac.cn (Xu MN); yalongjiang@whu.edu.cn (Jiang YL); zhaoahu19@mails.ucas.ac.cn (Zhao AH); xlshi@whrsm.ac.cn (Shi XL); ypli@whrsm.ac.cn (Li YP)

Yandy Scientific Press

3080-8812
Received Jan. 3, 2026; revised Jan. 10, 2025; accepted Jan. 26, 2026; available online Feb. 16, 2026.

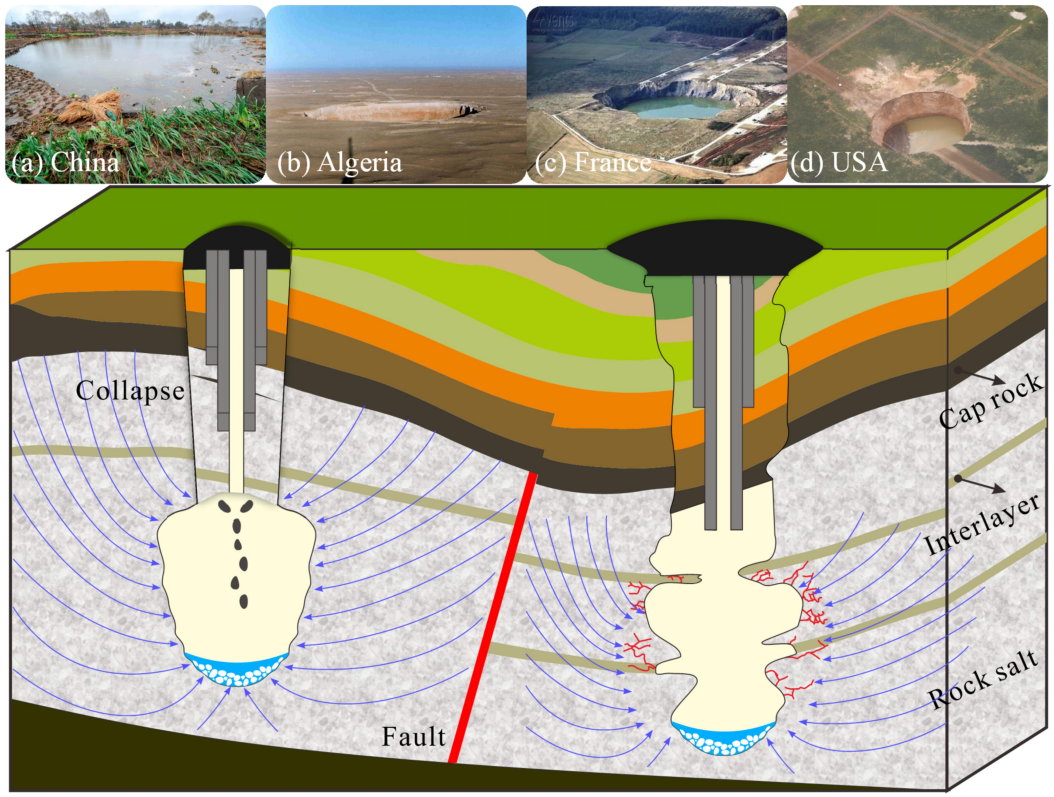

Fig. 1 Some typical salt mine collapse disasters around the world

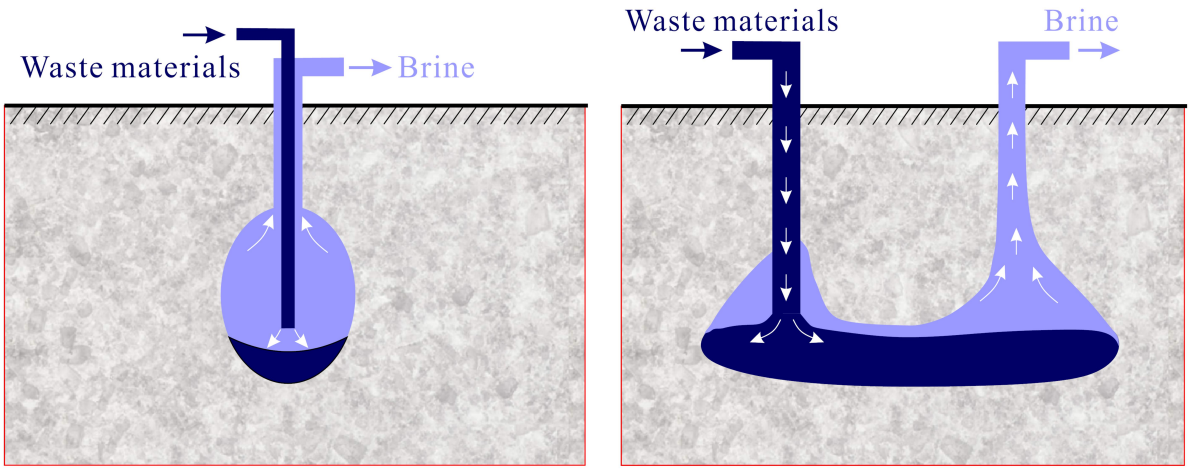

(a) Single salt cavern (b) Horizontal salt cavern

Fig. 2 Schematic diagram of alkali slag backfilling in salt caverns

center of the subsidence was circular, with a diameter of about 50 meters and a depth of approximately 5 meters. The subsidence occurred within the middle range of a pair of convection mining wells, with a well spacing of 330 meters. In 2006, ground subsidence also occurred at the Dingyuan Salt Mine in Anhui, China, with a subsidence area in the shape of an ellipse (Zhang et al., 2018, 2019), measuring 120 meters in length and 85 meters in width, covering approximately 7800 m^2. The cause of the subsidence was the excessive density of mining wells and prolonged mining activities, which led to the formation of large mined-out areas underground. This caused the salt roof to lose its support, resulting in collapse and ground subsidence. In 2014, during mining operations at the Longgui Salt Mine in Guangzhou, China, significant ground subsidence occurred, with a relatively fast subsidence rate (Zhang et al., 2024, 2020). A total of 36 cracking issues were identified within the affected mining area, including surface and road cracks and cracks in building facades, covering an area of about 0.95 km^2. Similar ground subsidence risks have also been reported in salt rock mines worldwide, including at Cerville-Buissoncourt and

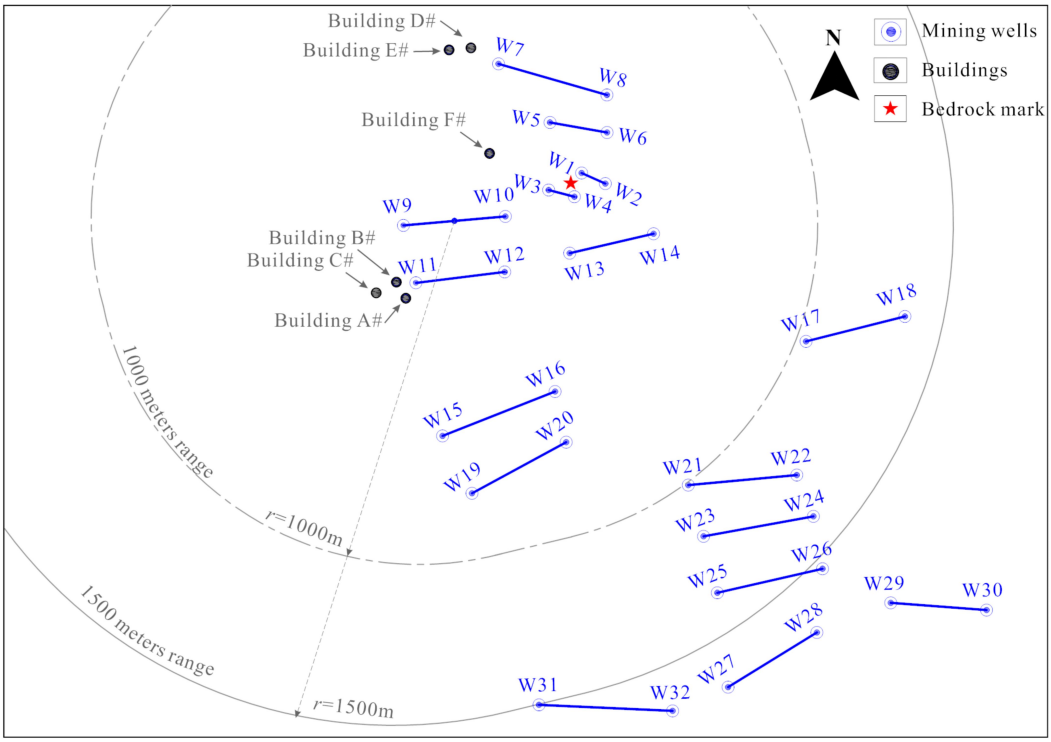

Fig. 3 Location information of salt mining wells and surrounding buildings

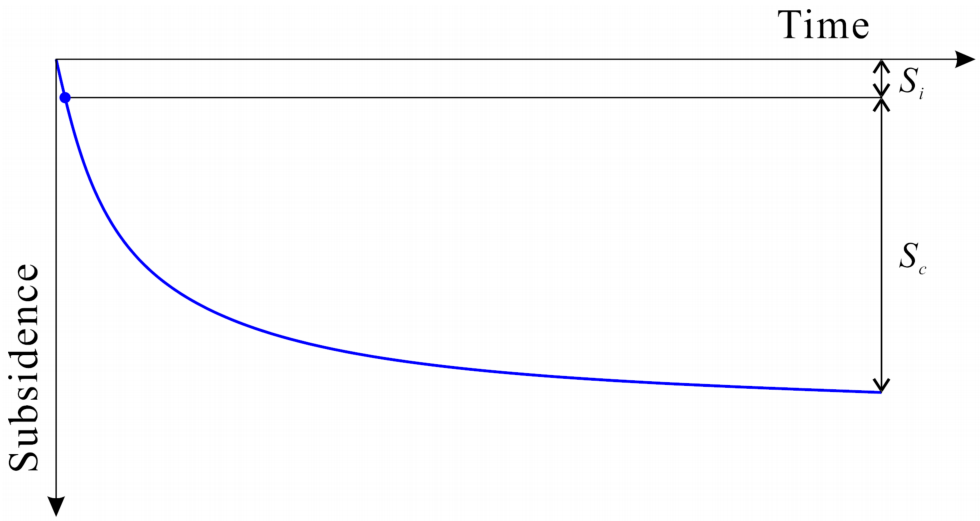

Fig. 4 The main components of surface subsidence in salt mines

Gellenoncourt in France, Texas and Louisiana in USA, Haoud Berkaoui in Algeria (Bérest, 2017; Daupley et al., 2010).

Salt mine collapses disasters around the world primarily occur in abandoned mining areas that have not received adequate attention, in mines with a depth of less than 500 meters, or in mines where mining activities have not been carried out according to design specifications. Collapses are rarely seen in operational salt cavern energy storage facilities. This is because salt caverns are underground spaces left behind by solution mining of salt mines, can effectively reduce the stress difference between the cavern and the surrounding strata when used for energy storage (Wan et al., 2023; Warren, 2016; Yang et al., 2023). This helps limit creep shrinkage of salt cavern, thereby reducing ground subsidence in the mining area.

In addition, for salt caverns that cannot be used for energy storage, such as deformed caverns with poor stability, small caverns with poor economic viability, or leaky caverns with poor sealing, backfilling with waste materials can be used to suppress cavern shrinkage (Fig. 2). This approach has been widely accepted and applied in many engineering projects, such as the Holford Salt Mine in Manchester, UK, the Moss Bluff Salt Mine in the USA, and the Longgui Salt Mine in Guangdong, China, as well as the Huai'an Salt Mine in Jiangsu, China (Ji et al., 2014; Langer, 1993; Shi et al., 2015; Xu et al.,

2014; Yang et al., 2021).

Utilizing salt cavern for energy storage and waste disposal not only addresses the problem of ground subsidence in salt mining areas but also brings new opportunities for the sustainable utilization and development of salt mine. Some research has already been conducted on the interaction between backfilled alkali slag and salt caverns. Xu et al. conducted a study on the mechanical properties of alkali slag and analyzed its impact on creep shrinkage of salt cavern (Xu et al., 2012). Li et al. investigated the compaction mechanism and inhibition effect of insoluble materials within salt cavern, and analyzed the long-term stability of gas injection and extraction in slag-filled salt caverns (Li et al., 2022, 2023). Furthermore, some scholars have proposed phenomenological viscoelastic models of surface subsidence based on the shrinkage behavior of single and dual caverns (Chen et al., 2022; Ye et al., 2022). However, due to the limitations of theoretical and experimental research, there is currently limited reporting on the effects of dynamic salt mining and alkali slag backfilling on surface subsidence.

This study takes 32 brine extraction wells from a real mining area in China as the research object. It considers the dynamic mining of underground salt cavern clusters and the dynamic backfilling of alkali slag, among other factors, to establish a theoretical analysis model. The study combines field monitoring data to analyze and predict surface subsidence in the mining area, and assess the safety and stability of nearby buildings. This research reveals the suppression mechanism of backfill alkali slag on creep shrinkage of salt cavern, and demonstrates its feasibility in the management of geological disasters in mining areas. The findings can provide valuable references and guidance for similar engineering projects, not only in salt mines but also in coal mines, metal mines, and other types of mineral resources.

2 Mechanism and influencing factors of surface subsidence in salt mines

2.1 Engineering geology overview

The salt mine studied is located in the eastern coastal region of China. After over 30 years of mining, the underground caverns formed in the salt mine area are vast. Preliminary estimates suggest that the underground space of the salt caverns covers an area of approximately 261,000 square meters, with a volume exceeding 20 million cubic meters, indicating significant potential for underground space resource utilization and a promising outlook for its future development. Based on drilling data, the stratigraphy in the salt mine area from bottom to top, of the Upper Cretaceous Pu'kou Formation (K2P) and Chishan Formation (K2C), the Upper Tertiary Yancheng Group (Ny), and the Quaternary Dongtai Formation (Qd). The salt-bearing strata in the block section are mainly composed of clastic rocks, sulfate rocks, and rock salt.

The structural types of the salt sequence can be divided as follows: clastic rock type-where the top and bottom of the salt layer consist of siltstone, mudstone, etc.; sulfate rock type-where the top and bottom of the salt layer are composed of gypsum rock and anhydrite; mixed type-where the top and bottom of the salt layer consist of a combination of these two types of rocks. The dip angle of the salt mine strata gradually decreases from the basin edge toward the basin center, with the dip angle at the basin edge generally ranging from 3 degrees to 10 degrees, and locally up to 15 degrees. Near the center of the basin, the strata are nearly horizontal, with a dip angle generally varying between 1 degree and 4 degrees. The lateral extent of the strata is controlled by the basin morphology, with the overall strike direction being northeastward, tilting slightly southward or south-southwestward.

The rock salt in the mining area has a low grade, with the insoluble content accounts for as high as 80%. According to the regulations in China and Europe (Belgian-Standards, 1998; National-Energy-Administration-of-China, 2011), it is not suitable for constructing salt cavern energy storage. Considering the overall stability and safety of the mining area, an alkali slag filling method for solution mining has been adopted. This method involves injecting alkali slag into the salt cavern simultaneously with solution mining once a certain depth is reached. This approach not only enhances the overall stability of the mining area but also addresses the disposal issue of waste slag and alkali slag. Due to the advantages of this technology, it has been applied in the Holford salt cavern in Manchester, UK, the Moss Bluff salt cavern in the USA, and the Shuanghuan salt cavern in Hubei, China, as well as the Huai'an salt cavern in Jiangsu, China, with promising prospects (Warren, 2006; Xu et al., 2014). The impact of backfill alkali slag on the subsidence of the mining area will be discussed in detail in Section 2.3.

As shown in Fig. 3, there are currently 16 pairs of salt mining wells in the target mining area. Among them, W1, W2, W3, and W4 have been connected and mining has ceased due to their small spacing, and the alkali slag backfilling completed. Salt mining wells W5-W6 and W7-W8 stopped in 2023, and alkali slag backfilling has been completed. The remaining salt mining wells are still being mined and alkali slag backfilling is being carried out simultaneously. According to the current annual mining rate, it is expected that most of the salt mining wells will reach the designed mining height by 2052, at which point mining will cease.

2.2 Mechanism of surface subsidence

The subsidence mechanism in salt mining is similar to that in coal mining and other types of mining. It can be summarized as the instability of the mining pillar, roof collapse, cavern collapse, or strata failure, all of which lead to varying degrees of surface subsidence or sinkholes. Due to the use of solution mining method, the surface subsidence of salt mine also has its distinct characteristics, such as surface subsidence being frequently accompanied by phenomena like brine outcrop and groundwater system pollution.

As shown in Fig. 4, surface subsidence in salt mines consists of two main components: 1) The instantaneous deformation induced by the release of ground stress; 2) The continuous deformation during the solution mining and operating stage due to creep of surrounding rocks in salt cavern (Scigata and Szafulera, 2020). The creep of surrounding rock leads to a gradual reduction in the volume of the salt cavern, and the volume loss in this process is ultimately reflected to the surface

through the strata.

For a single salt cavern, assuming that the surface subsidence profile follows a Gaussian function, the subsidence curve can be expressed as (Lyu et al., 2024):

$$W_e(r) = W_{\max} \cdot \exp\left(-\pi \frac{r^2}{R_0^2}\right) \quad (1)$$

where $W_{\max}$ represents the sedimentation at the subsidence center, r represents the radial distance, R_0 denotes subsidence influence radius.

The surface subsidence caused by double salt caverns and horizontal salt cavern can be calculated using the superposition principle based on the theoretical model of a single salt cavern, and several theoretical models have been proposed for this purpose (Ye et al., 2022). However, this analytical approach is not applicable to group caverns, as the number of caverns is large and the influence range is extensive. Additionally, many factors affect the subsidence, such as pressure transfer between caverns, creep shrinkage and backfill materials, making it difficult to achieve accurate results through theoretical analysis alone. For surface subsidence analysis of salt cavern clusters, it is typically necessary to combine numerical simulations with field monitoring data to more accurately assess the surface subsidence.

2.3 Influencing factors

Surface subsidence in mining areas is closely related to the long-term creep of the surrounding rock in salt caverns, hence factors directly affecting the shrinkage of salt cavern will indirectly influence surface subsidence (Babaryka and Benndorf, 2023). These factors can generally be classified into two categories: external factors and internal factors. External factors include: the depth of the storage, ground stresses, formation temperature, operating pressure and duration, the geometry of salt cavern, and backfill materials. Internal factors include: lithology, creep behavior of the surrounding rock, and the creep stage.

It is important to note that the majority of rock salts in China are lacustrine deposits, which have low grades and high impurity content (Liu et al., 2020). After dissolution, a significant amount of insoluble material remains. During the solution mining process, these insoluble materials settle at the bottom of the cavern, occupying a large portion of the cavern volume. As a result, the storage efficiency of such rock salt formations is low, and their economic viability is poor. This is exactly the case with the salt mine studied in this paper.

However, the insoluble materials provide more support to the cavern walls than gas and brine, which contributes to the stability of the salt cavern. Inspired by this concept, a new technology for fill-based solution mining in salt mines has been proposed in the engineering field, as shown in Fig.5. Alkali slag is used as the filling material to backfill the mined salt caverns after solution mining. Once the salt cavern is filled to a designed position, the solution mining is resumed. This process involves a cyclic operation of solution mining and filling alkali slag. As the amount of filling increases and time progresses, the filling material settles, consolidates, and densifies under the influence of gravity and compression. Its bulk modulus and shear modulus continuously increase, forming a filling body with a certain strength that supports the salt roof and cavern walls of the mined salt cavern. The physical and mechanical parameters of alkali slag before backfilling are shown in Tab.1.

The improvement of the cavern stability by backfill alkali slag is primarily achieved by inhibiting the final volume shrinkage of the salt cavern. The main reasons are:

(1) The backfill materials have a higher density than that of gas and brine, providing greater horizontal support.

(2) The backfill materials have a certain strength, which can partially suppress the volume shrinkage of the salt cavern.

(3) The backfill materials are continuously compressed and consolidated, further restricting cavern shrinkage.

2.4 Theoretical analysis model

Considering the inhibitory effect of backfill alkali slag on salt cavern shrinkage, the shrinkage trend of a salt cavern can be divided into the following three stages:

(1) Instantaneous deformation in the early stage of solution mining.

(2) Continuous creep shrinkage during the solution mining.

(3) Shrinkage inhibition and cessation after well sealing.

This shrinkage trend is closely related to the deformation behavior of the surrounding rock and the backfill alkali slag, and a new calculation model needs to be proposed. For this purpose, a conceptual model simultaneously considers the elastic-plastic-viscos properties of both the rock salt and the backfill alkali slag, as well as their combined effects.

In the first stage, before the alkali slag is backfilled, the instantaneous shrinkage of the cavern is solely related to the elastoplastic deformation of the surrounding rock, which can be described using the Mohr-Coulomb constitutive model (Chen et al., 2023; Xu et al., 2019).

$$f(\sigma_1, \sigma_2, \sigma_3) = \frac{1}{2}(\sigma_1 - \sigma_3) + \frac{1}{2}(\sigma_1 + \sigma_3)\sin\varphi - C \cdot \cos\varphi \quad (2)$$

where σ_1 and σ_3 represent the first and third principal stresses, C and ϕ represent the cohesion and internal friction angle of material.

In the second stage, solution mining and alkali slag backfilling are carried out simultaneously. The continued shrinkage of the cavern is primarily related to the creep deformation of the surrounding rock. Therefore, the surrounding rock deformation is described using the Norton-Hoff constitutive model. At this stage, the alkali slag is not yet consolidated and behaves like a slurry, with a gradient pressure applied according to its density (Gwiazda et al., 2015).

$$\frac{\partial \varepsilon_{cp}}{\partial t} = A\left(\frac{\sigma_{mises}}{\sigma_{ref}}\right)^n \exp\left(-\frac{Q}{RT}\right) \quad (3)$$

$$\sigma_{\text{mises}} = \sqrt{3J_2} \quad (4)$$

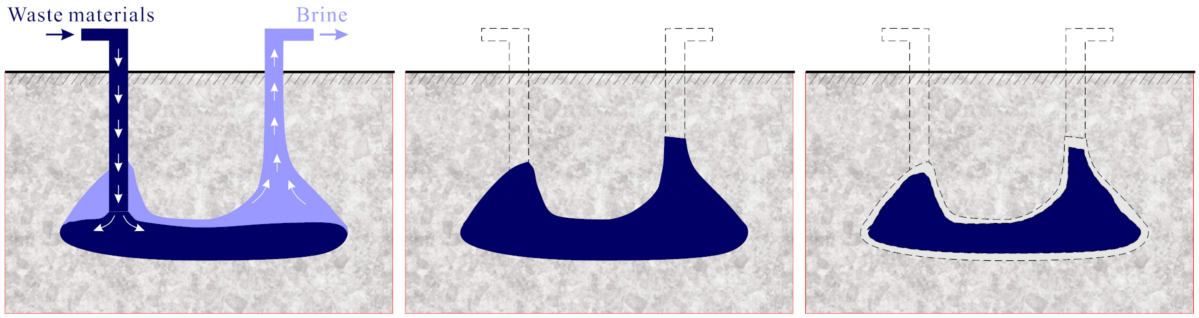

(**a**) Solution mining stage (**b**) Closure stage (**c**) Consolidation stage

Fig. 5 The physical state of backfill alkali slag at different stages and its effect on volume shrinkage of salt cavern

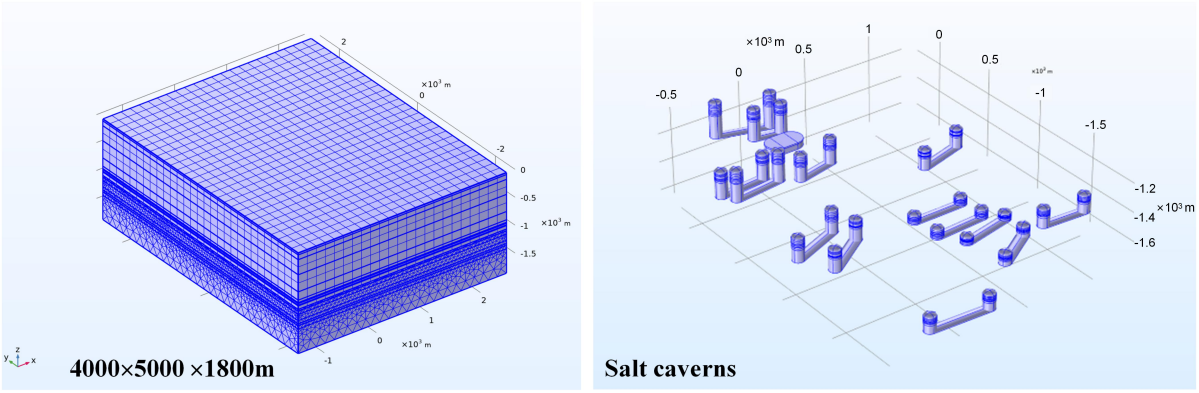

(**a**) 3D geological model (**b**) Salt caverns

Fig. 6 Three-dimensional numerical model and spatial distribution of salt caverns

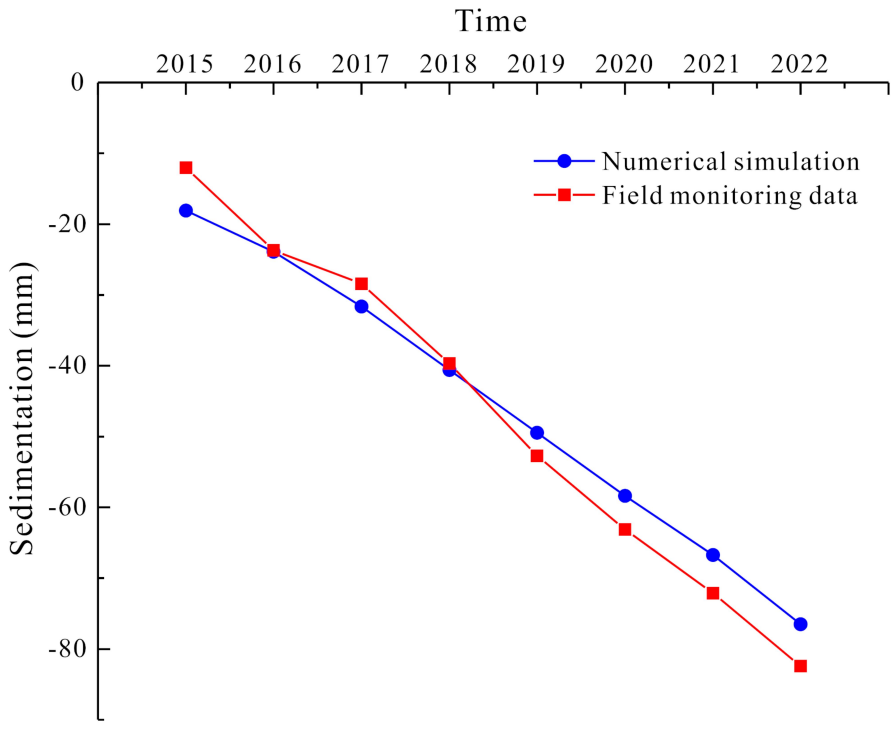

Fig. 7 Comparisons of numerical simulation and field monitoring data for BR1

Tab. 1 Physical and mechanical parameters of alkali slag before backfilling

Initial porosity ratio[1]	Initial density[kg. m^{-3}]	Initial moisture content[%]	Liquidity Index [1]
3.0	1323	214	>1

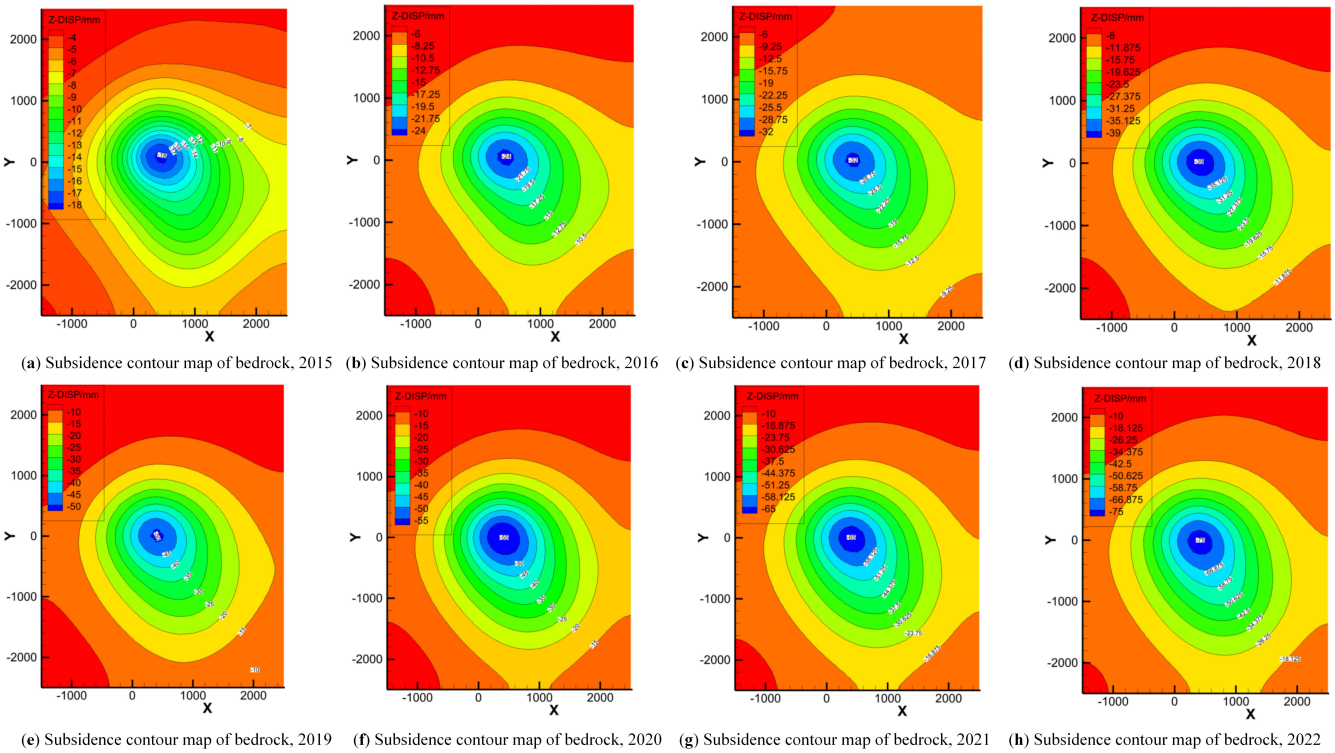

(**a**) Subsidence contour map of bedrock, 2015 (**b**) Subsidence contour map of bedrock, 2016 (**c**) Subsidence contour map of bedrock, 2017 (**d**) Subsidence contour map of bedrock, 2018

(**e**) Subsidence contour map of bedrock, 2019 (**f**) Subsidence contour map of bedrock, 2020 (**g**) Subsidence contour map of bedrock, 2021 (**h**) Subsidence contour map of bedrock, 2022

Fig. 8 Subsidence contour maps of bedrock marker from 2015 to 2022

where ε_{cp} denotes creep strain, A and n are the creep rate coefficient and stress exponent which can be obtained through creep experiments, σ_{mises} and σ_{ref} are Von Mises stress and reference stress 1 MPa, J_2 and Q denotes second deviatoric stress invariant and creep activation energy.

In the third stage, solution mining has been completed, and the cavern is filled with the backfill alkali slag and insoluble materials. The "hardening" effect of the two materials begins to take effect. The surrounding rock deformation continues to be described using the Norton-Hoff constitutive model, while the alkali slag is modeled using a modified Cam-Clay constitutive model to characterize its consolidation behavior (Hashash and Whittle, 1992).

$$f(p',q') = \left(p' - \frac{p'_0}{2}\right)^2 + \left(\frac{q'}{M}\right)^2 - \left(\frac{p'_0}{2}\right)^2 \tag{5}$$

where p' and q' are the octahedral normal stress and shear stress, M is the slope of the critical state line (CSL) in p'-q' stress space, p'_0 represents hardening function.

The explained constitutive model is triggered in stages and is suitable for describing the time-dependent mechanical behavior of the surrounding rock and the consolidation behavior of the alkali slag.

3 Subsidence history and reproduction in mining areas

3.1 Subsidence investigation

The mining area has a bedrock marker (BR1) located 400 meters below the surface where four connected wells (W1-W2, W3-W4) (Fig. 3). The subsidence monitoring data from 2015 to 2022 show that the annual subsidence of the BR1 ranged from 4.7 mm to 12.0 mm, with a cumulative subsidence of 82.4 mm. As shown in Fig. 3, there are multiple high-rise buildings around the mining area, and subsidence monitoring data have been collected for six buildings. Buildings A#, B#, and C# are located to the southwest of the BR1. Building A# experienced a cumulative subsidence of 13.74 mm between March 2014 and August 2015, with an average annual subsidence of 9.67 mm/year. Building B# had a cumulative subsidence of 10.55 mm from October 2018 to June 2020, with an average annual subsidence of 6.32 mm/year. Building C# had a cumulative subsidence of 8.96 mm from September 2018 to June 2020, with an average annual subsidence of 5.12 mm/year. Buildings D#, E#, and F# are located to the northwest of the BR1. Building D# had a cumulative subsidence of 18.57 mm between October 2018 and July 2020, with an average annual subsidence of 10.61 mm/year. Building E# experienced a cumulative subsidence of 15.64 mm from October 2018 to July 2020, with an average

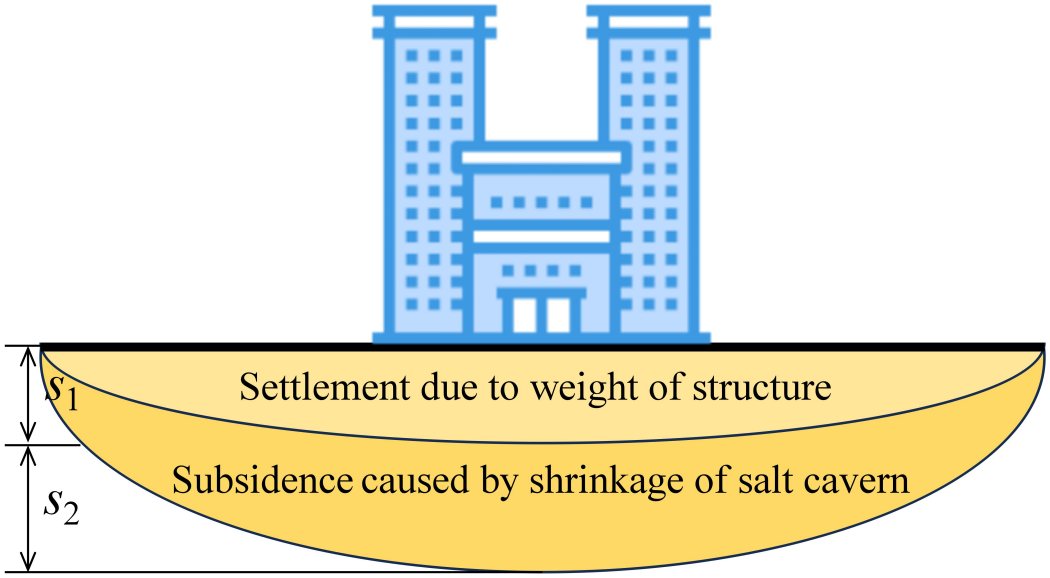

Fig. 9 The composition of foundation deformation for newly constructed buildings on the surface of the salt mining area

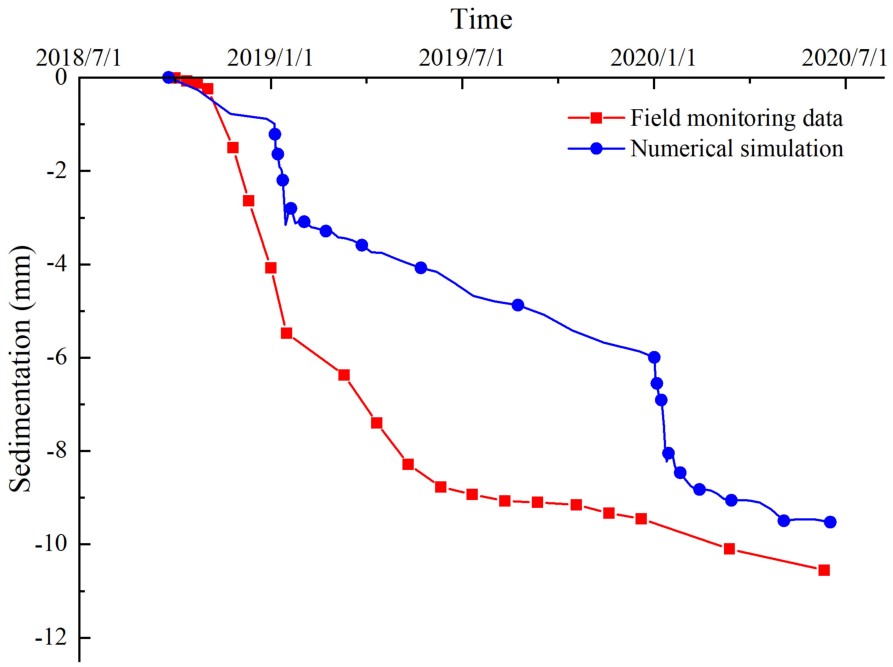

Fig. 10 Comparisons of numerical simulation and field monitoring data for building B#

annual subsidence of 8.94 mm/year. Building F# had a cumulative subsidence of 13.40 mm between September 2014 and July 2016, with an average annual subsidence of 7.32 mm/year.

3.2 Parameter inversion

Geological data indicate that the lithology of the overlying strata (referring to the rock formations above the rock salt) across various well groups in the mining area is relatively consistent. From top to bottom, the sequence consists of clay, sandy clay, fine sand, mudstone, gravel layer, argillaceous siltstone, and silty mudstone. Core samples from the strata near the mining area have been collected, and the corresponding calculation parameters, such as elastic modulus, Poisson's ratio, cohesion, internal friction angle and tensile strength were obtained through laboratory tests including uniaxial compression, triaxial compression, and creep testing.

The research results demonstrated that the size of the salt caverns, creep time, and the mechanical and creep parameters of the surrounding rock have a decisive influence on cavern shrinkage and surface subsidence. Although extensive mechanical tests on rock salt and mudstone interlayers have been conducted and relevant parameters have been obtained, discrepancies between

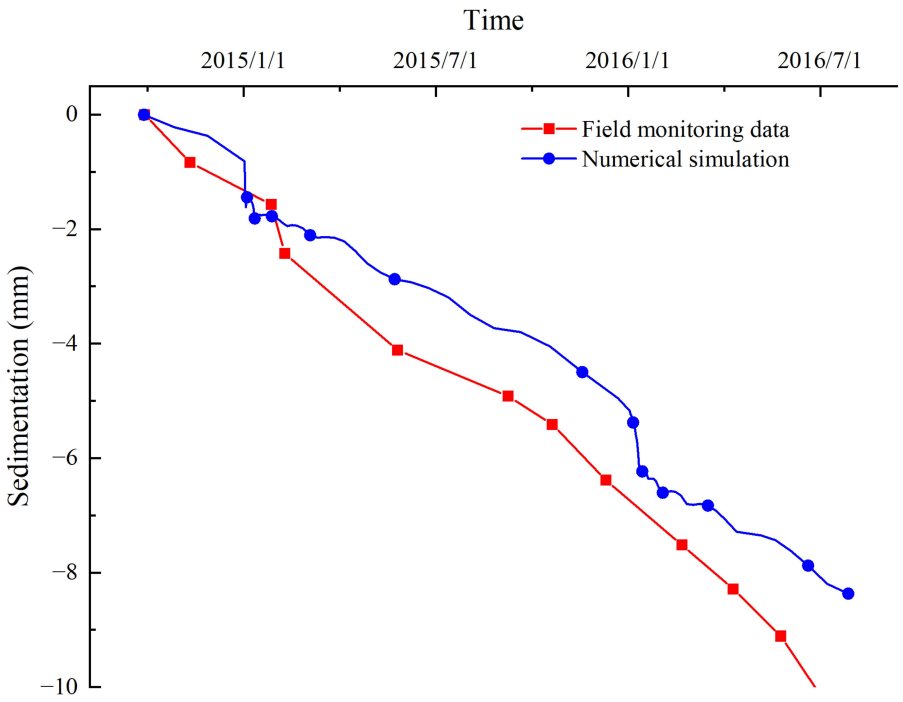

Fig. 11 Comparisons of numerical simulation and field monitoring data for building F#

experimental results and real-world conditions arise due to the complexity of underground engineering and the limitations of laboratory tests. Directly applying these experimental parameters for analysis often fails to reproduce the actual subsidence and deformation patterns observed in the mining area. Factors contributing to these discrepancies include core sampling disturbances, changes in the stress field, size effects, and rock anisotropy, among others.

To accurately reproduce the large-scale subsidence patterns in the mining area, a parameter inversion study was conducted. The inversion analysis was based on field monitoring data, cavern measurement data, brine extraction data, and laboratory test results to ensure its scientific validity and rationality. The parameter inversion focused on the collected subsidence monitoring data and results from laboratory uniaxial, triaxial, and creep tests. Through more than 30 iterations of inversion analysis and parameter corrections and incorporating the findings of relevant researchers (Yang et al., 2013; Zhang et al., 2017), the required calculation parameters for the numerical simulation of subsidence in the target mining area were ultimately determined, as shown in Table 2.

3.3 Deformation reproduction

3.3.1 Numerical modeling and boundary conditions

The three-dimensional geological model spans from the surface layers to the bottom layers, consisting of a total of 17 layers (Tab.1). Considering that the salt cavern clusters have a large impact on ground subsidence, the model was designed to eliminate boundary effects by placing the lateral edges of the model at least 10 times the radius of the nearest cavern, approximately 450 meters. The final model size was determined to be 4000 m × 5000 m × 1800 m (length × width × height). The model primarily uses tetrahedral and hexahedral meshes, with refined meshing applied to areas near the salt caverns. Fixed constraints were applied at the bottom of the model, roller constraints on the surrounding sides of the model, and a free surface was set at the top of the model. Fig.6 shows the three-dimensional geological model of the target mining area, which clearly shows the stratigraphic grouping and the number and spatial distribution of salt caverns.

3.3.2 Deformation reproduction of bedrock marker

Based on the proposed theoretical analysis model and aided by numerical simulation, the subsidence patterns in the mining area from 2015 to 2023 were reproduced. Each subsidence analysis dynamically adjusted the cavern size according to the brine extraction data, while also utilizing the deformation data from the previous year, and so on, up to 2023. Fig. 7 shows the comparison between the numerical calculation results of subsidence at the bedrock marker (BR1) and the field monitoring data. The cumulative subsidence of the BR1 increases linearly with time. The numerical subsidence results for the period from 2015 to 2022 are as follows: -18.10 mm, -23.91 mm, -31.61 mm, -40.61 mm, -49.45 mm, -58.36 mm, -66.71 mm, and -76.51 mm, with an average annual subsidence of 9.56 mm. Compared to the field monitoring data for the same period at the BR1, the errors of the numerical simulation from 2016 onwards are: 0.89%, 11.29%, 2.30%, 6.17%, 7.51%, 7.47%, and 7.15%, with the overall error being relatively small.

The contour maps (Fig. 8) show that the subsidence center of the mining area is located near four connected wells (W1, W2, W3, and W4), extending towards the lower right corner (southeast direction). This subsidence trend is closely related to the density of underground salt caverns and the connectivity of the four wells. Under the same creep time, the more caverns that

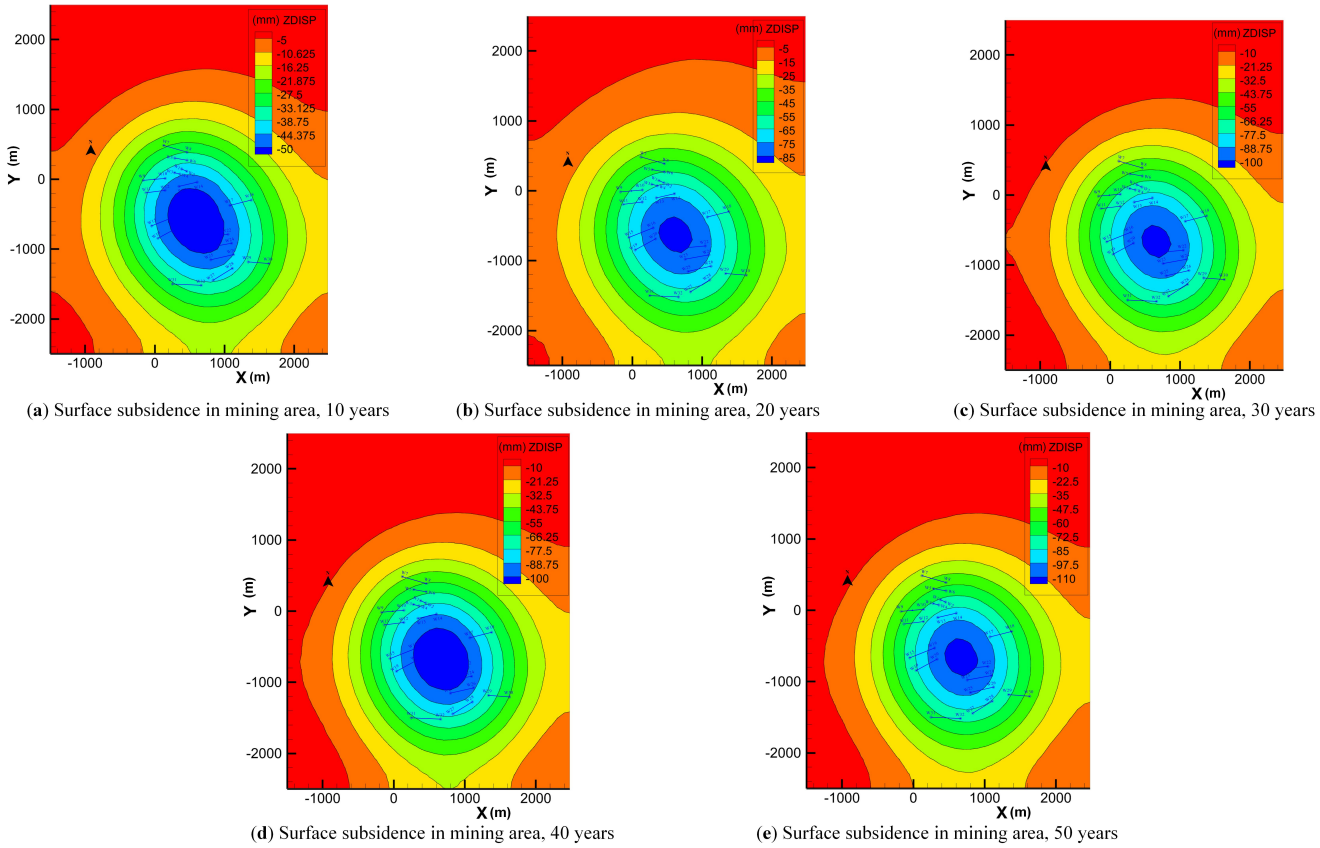

(**a**) Surface subsidence in mining area, 10 years (**b**) Surface subsidence in mining area, 20 years (**c**) Surface subsidence in mining area, 30 years

(**d**) Surface subsidence in mining area, 40 years (**e**) Surface subsidence in mining area, 50 years

Fig. 12 Contour maps of surface subsidence prediction in mining areas from 2024 to 2073

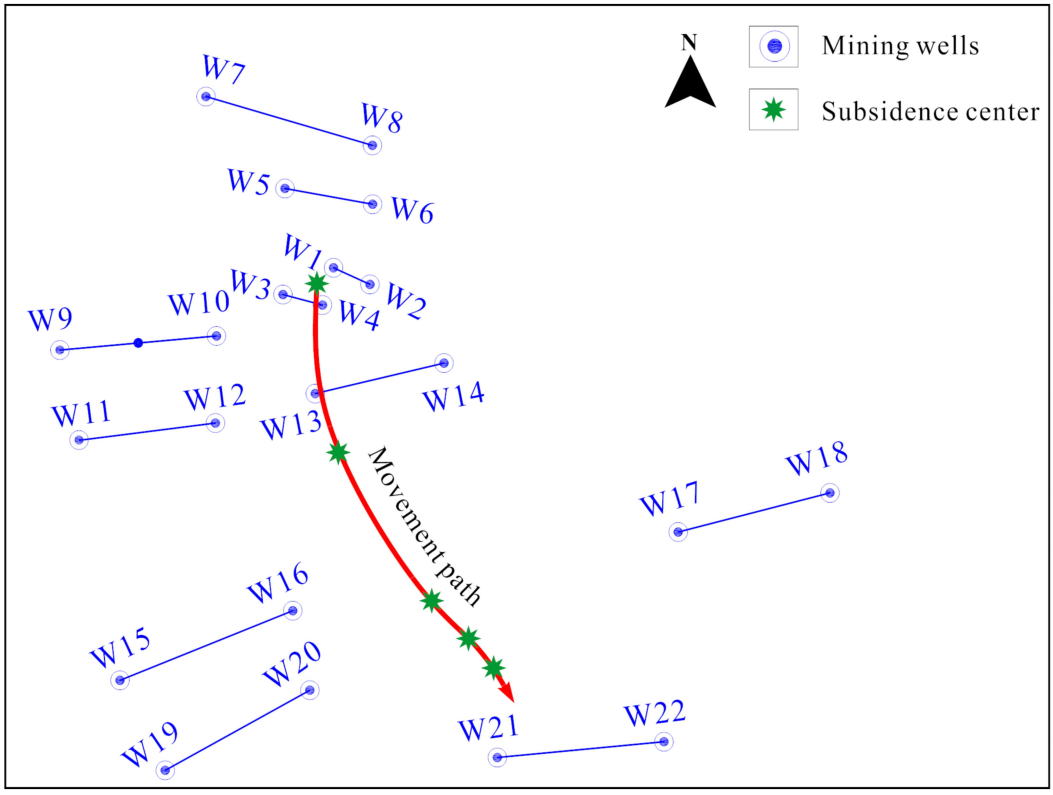

Fig. 13 Movement path of surface subsidence center of the mining area from 2015 to 2073

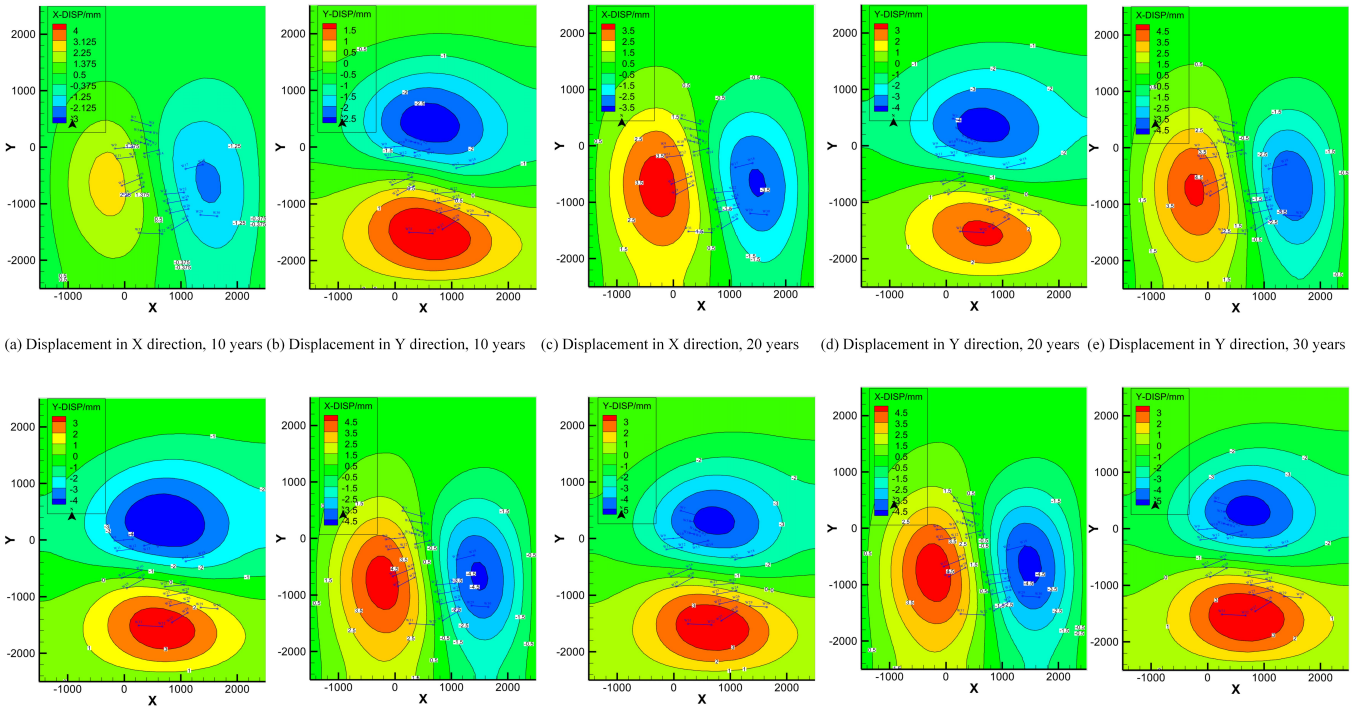

(a) Displacement in X direction, 10 years (b) Displacement in Y direction, 10 years (c) Displacement in X direction, 20 years (d) Displacement in Y direction, 20 years (e) Displacement in Y direction, 30 years

(f) Displacement in Y direction, 30 years (b) Displacement in X direction, 40 years (c) Displacement in Y direction, 40 years (d) Displacement in X direction, 50 years (e) Displacement in Y direction, 50 years

Fig. 14 Horizontal surface displacement of the mining area from 2024 to 2073

Tab. 2 Physical and mechanical parameters of formation for the numerical simulation of subsidence in the target mining area

Lithology from top to bottom	Thickness [m]	Young modulus [GPa]	Poisson's ratio	Cohesion [MPa]	Internal friction angle [°]	Tensile strength [MPa]	Creep rate coefficient [10^{-6} a^{-1}]	Stress exponent
Clay	31.2	0.01	0.30	0.02	15.00	0.0020	—	—
Sandy clay, fine sand	85.8	0.02	0.30	0.01	21.66	0.0012	—	—
Mudstone, gravel layer	269.5	1.65	0.24	0.15	21.94	0.18	—	—
Siltstone	306.5	5.24	0.24	0.55	36.35	0.66	—	—
Mudstone (Cap rock)	148.09	6.22	0.30	3.22	36.38	0.66	—	—
Rock salt 1	44.5	5.56	0.29	3.78	37.06	0.63	0.86×10^{-6}	3.55
Mudstone 1	18.48	6.22	0.30	3.22	36.38	0.66	0.05×10^{-6}	3.41
Rock salt 2	28.08	5.48	0.29	3.85	37.14	0.63	0.97×10^{-6}	3.50
Mudstone 2	13.63	6.22	0.30	3.22	36.38	0.66	0.05×10^{-6}	3.33
Rock salt 3	59.92	5.34	0.29	3.97	37.29	0.62	1.14×10^{-6}	3.52
Mudstone 3	33.69	6.09	0.30	3.33	36.52	0.65	0.21×10^{-6}	3.17
Rock salt 4	60.01	5.54	0.29	3.79	37.08	0.63	0.89×10^{-6}	3.55
Rock salt 5	109.1	5.08	0.29	4.18	37.55	0.61	1.46×10^{-6}	3.47
Rock salt 6	56.5	5.81	0.30	3.57	36.81	0.64	0.56×10^{-6}	3.48
Rock salt 7	36.3	5.05	0.29	4.21	37.58	0.61	1.50×10^{-6}	3.55
Rock salt 8	58.7	5.72	0.30	3.65	36.90	0.64	0.68×10^{-6}	3.51
Underlying strata	440	5.44	0.29	3.88	37.18	0.63	1.48×10^{-6}	3.50

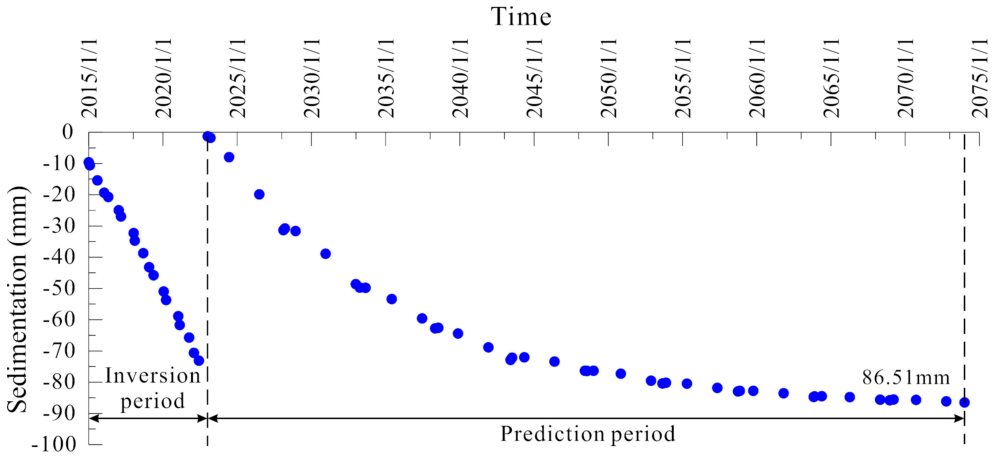

(a) The accumulated deformation during the inversion period (2015–2023) are reset to zero

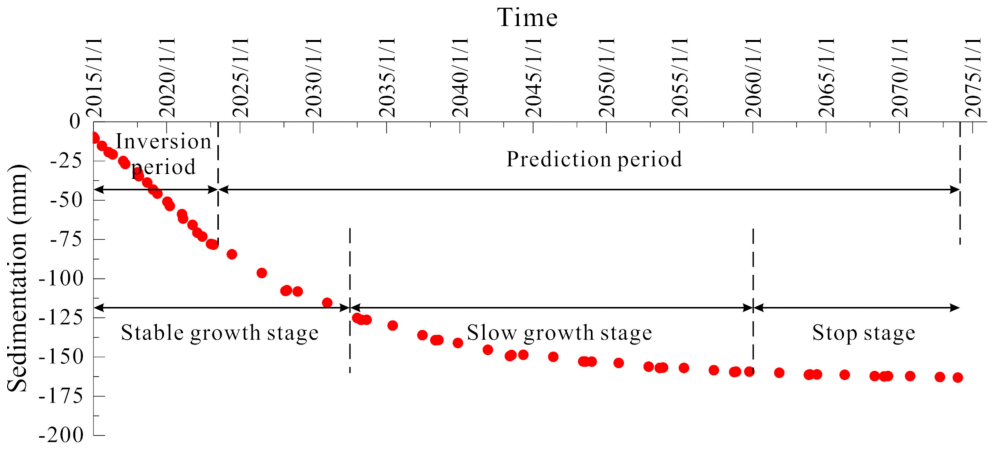

(b) The accumulated deformation during the inversion period (2015–2023) are not reset to zero

Fig. 15 Full-stage subsidence variation curves of the bedrock marker (BR1) with and without considering the reset of subsidence to zero

are being mined and the larger the cavern volume, the greater the subsidence in both the formations and the ground surface. The overall subsidence trend in the contour maps is consistent with the actual situation.

3.3.3 Deformation reproduction of buildings

The collected data was extracted from the subsidence monitoring report during the main structure construction of the buildings. During the construction of the main structure, the underground salt cavern continued to undergo volume shrinkage, so the subsidence data in the monitoring report primarily comes from two parts (Fig. 9):

(1) The increase in foundation pressure caused by the gradual construction of the main structure, leading to settlement deformation of the foundation soil;

(2) Ground subsidence induced by mining activities in the area and the volume shrinkage of the salt caverns.

To ensure the accuracy of the data comparison, the settlement caused by the construction of the building's main structure should be subtracted, making the data comparable. The settlement deformation of the first part can be calculated by the layered summation method. The calculation depth of foundation settlement is divided into several layers, the compression of each layer is calculated, and then sums them up. When calculating, the calculation depth of foundation settlement should first be determined based on the foundation load, base shape and size, as well as relevant soil parameters. The depth range for settlement calculation should then be divided into layers, followed by the calculation of the additional stress at the foundation base, as well as the average self-weight stress and additional stress at the top and bottom of each layer.

Considering the large amount of data collected for the buildings, and to avoid redundant analysis, building B# and building F# are selected as the analysis objects for model validation. Fig. 10 shows the comparison between the subsidence monitoring data (subtracting the foundation settlement caused by the construction of the building structure) of building B# during the

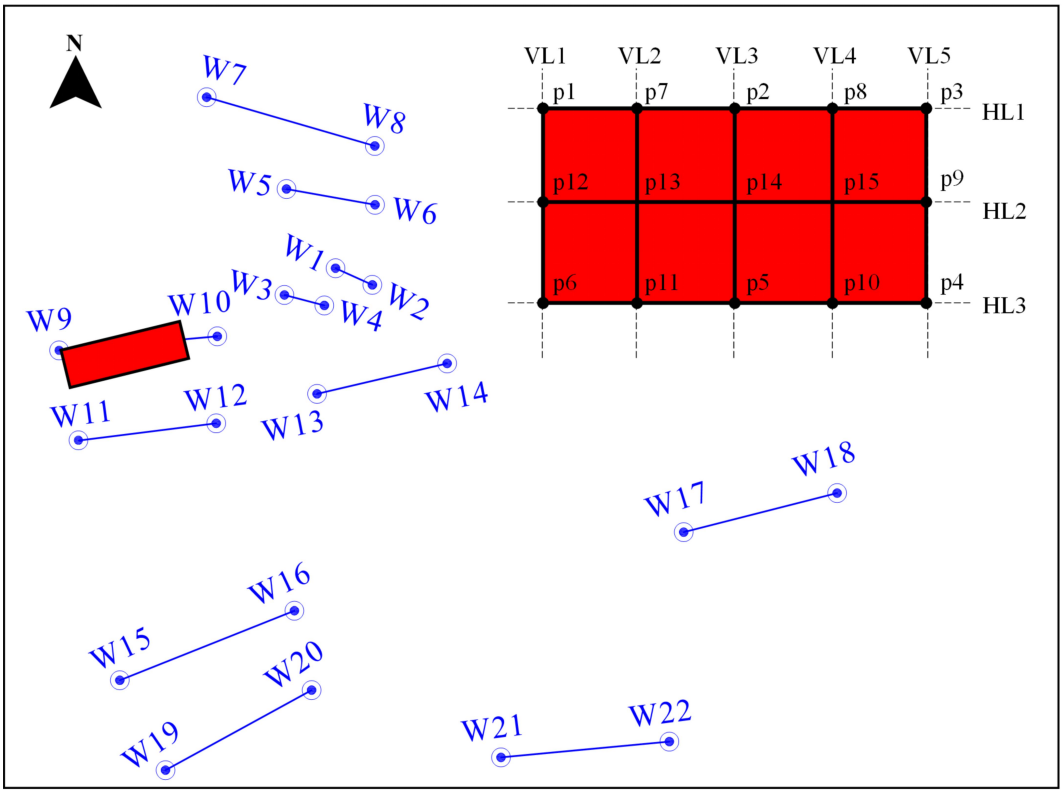

Fig. 16 The target plot information

monitoring period and the numerical simulation results. Their overall subsidence trends are highly consistent, with the subsidence amount gradually increasing over time and eventually stabilizing. Compared to the field subsidence monitoring curve, the numerical simulation results show sharp variations at the beginning of each year due to changes in the salt cavern volume. The final error is approximately 14.82%. Fig. 11 shows the comparison between the subsidence monitoring data (subtracting the foundation settlement caused by the construction of the building structure) and the numerical simulation results during the monitoring period of building F#. Their overall subsidence trends match well, with the final error being approximately 13.32%. The proposed theoretical model and analysis approach successfully reproduced the subsidence patterns of the strata in the mining area and the surrounding buildings. The overall error is relatively small, validating the applicability and accuracy of this model.

4 Prediction and analysis of long-term subsidence

The previous research results in this study have indicated that salt caverns continue to shrink under the differential stresses caused by ground stress and operating pressure, which have a certain impact on the safety of surrounding buildings and the ecological environment. Based on the previously established calculation model and the inversion parameters, this section considers the impact of backfill alkali slag in salt caverns on ground subsidence and conducts an analysis and prediction of the deformation patterns in the mining area over the next 50 years (building life).

4.1 Mining area subsidence

Before conducting long-term surface subsidence prediction and stability analysis for the mining area, all accumulated deformation and deformation rates during the inversion period (2015–2023) were reset to zero, with the time period starting from 2024 and ending in 2073. Fig. 12 shows the cumulative surface subsidence contour maps for the next 10, 20, 30, 40, and 50 years, with maximum subsidence values of -55.40 mm, -88.09 mm, -103.01 mm, -111.06 mm, and -114.21 mm, respectively. Using 10-year intervals as analysis nodes, the deformation rates for the maximum subsidence in the mining area are 5.54 mm/year, 3.27 mm/year, 1.49 mm/year, 0.81 mm/year, and 0.32 mm/year. One can see that due to the factors such as brine dissipation, salt cavern shrinkage, and the gradual compaction of the backfill alkali slag, the supporting pressure inside the salt cavern gradually increases and eventually reaches equilibrium with the formation stress. As a result, the subsidence rate significantly decreases with time, and the subsidence value of the mining area gradually diminishes, ultimately tends to stop.

Additionally, it can be clearly seen from the contour maps of surface subsidence prediction that the subsidence center (maximum subsidence) of the mining area has moved significantly. It moves from the near the four connected wells (W1-W2, W3-W4) in 2015 to the vicinity of Wells W21-W22 in 2073. The subsidence center moves overall in a southeastward direction, with a displacement of approximately 632.44 meters. The movement path is shown in Fig. 13. The movement of the subsidence center is primarily attributed to two factors:

(1) The subsidence prediction model takes into account the

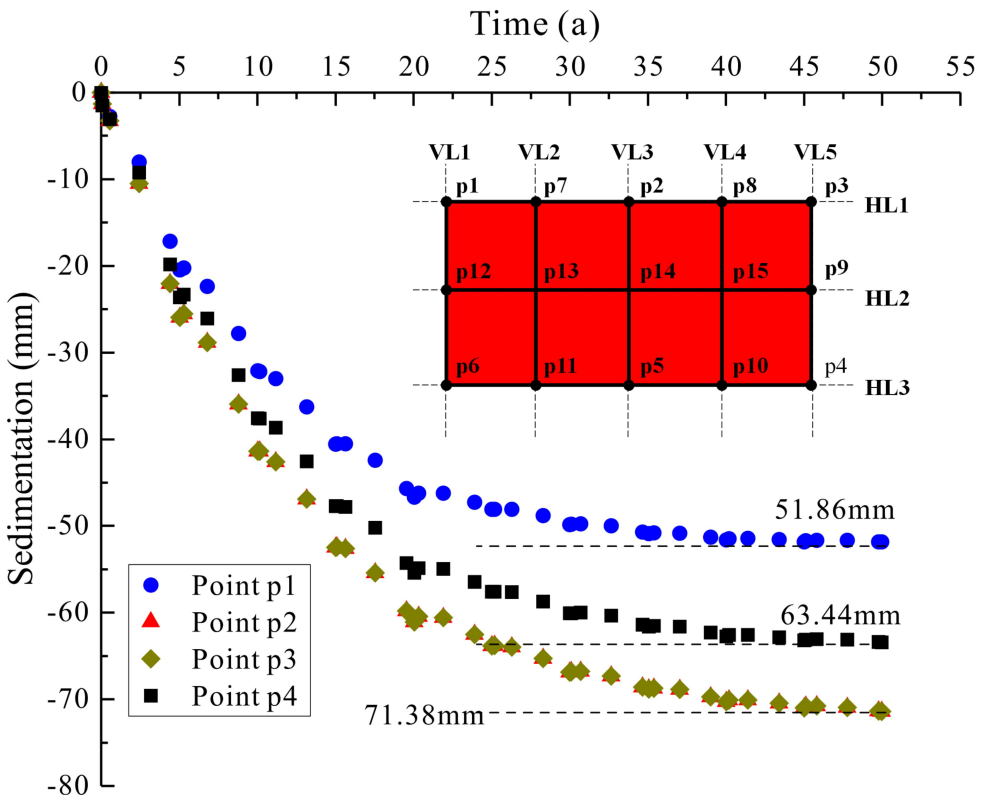

Fig. 17 The subsidence trend of the corner points of the plot from 2024 to 2073

dynamic mining of the underground salt caverns. Based on the currently collected brine extraction data, the seven pairs of wells in the upper mining area (W1-W14) will enter the well closure stage earlier.

(2) The backfill alkali slag in the salt caverns of the upper mining area plays a significant role in suppressing the cavern shrinkage, with the volume shrinkage of the cavern gradually slows down until it stops.

4.2 Horizontal deformation

Fig. 14 shows the cumulative displacement cloud maps in the X and Y directions at the surface of the mining area predicted based on the theoretical model. Since the subsidence cloud maps appear in the form of a settlement trough, the displacement of the ground surface in the X and Y directions exhibit symmetry, with the axis of symmetry located at the settlement center. The magnitudes of displacement in the X and Y directions are comparable, with the maximum horizontal displacement approximately 4% to 5% of the maximum subsidence. It can be concluded that salt mining has a certain impact on the surface deformation of the mining area, with the primary effect concentrated in the vertical direction..

4.3 Full-stage subsidence trend

The bedrock mark (BR1) is buried at a depth of -400 meters, and analyzing its subsidence pattern over the next 50 years has significant reference value for the long-term stability evaluation of the mining area. Fig. 15 show the subsidence variation curves for BR1 during the prediction period (2024–2073), with and without considering the reset of subsidence to 0.

The prediction results indicate that the subsidence of BR1 during the inversion period (2015–2023) increases linearly with time, with an average annual subsidence of 9.56 mm. Upon entering the prediction period, the previous subsidence will continue to exhibit linear growth, representing a stable growth phase, lasting for about 10 years. Subsequently, the growth rate of the subsidence begins to slow down, mainly due to the increase in brine pressure after well closure, and the compaction effect of the backfill alkali slag and insoluble materials within the salt caverns. It represents a slow growth phase lasting approximately 30 years. The final stage is the equilibrium phase, and the subsidence has almost no significant change over time. During this stage, the “hardening” effect of the backfill alkali slag and insoluble materials within the salt caverns plays a key role, lasting approximately 10 years. After 50 years, the cumulative subsidence of BR1 is expected to be 86.51 mm, with an average annual subsidence of 1.73 mm, a reduction of approximately 81.90% compared to the inversion period.

In summary, the full-stage subsidence trend of the mining area has three distinct stages. These stages correspond to the three phases of volume reduction in the salt cavern due to well closure and alkali slag backfilling:

(1) Stable growth stage. In this stage, the subsidence is primarily driven by the resistance of brine pressure and lateral pressure from sediment materials against the geological stress, resulting in approximately linear subsidence across the mining area. This stage follows the subsidence pattern observed during the inversion period.

(2) Slow growth stage. During this stage, some mining wells have already entered the closure phase, and the cavern contains

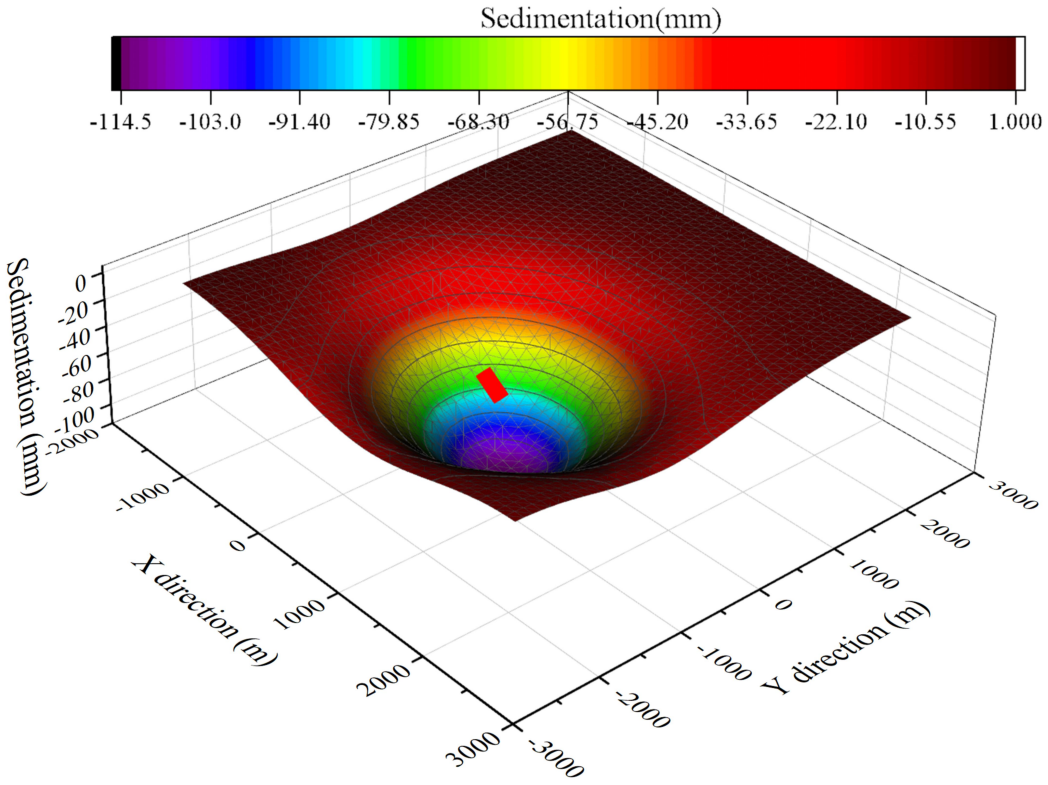

Fig. 18 Three-dimensional subsidence contour map of the mining area 50 years later

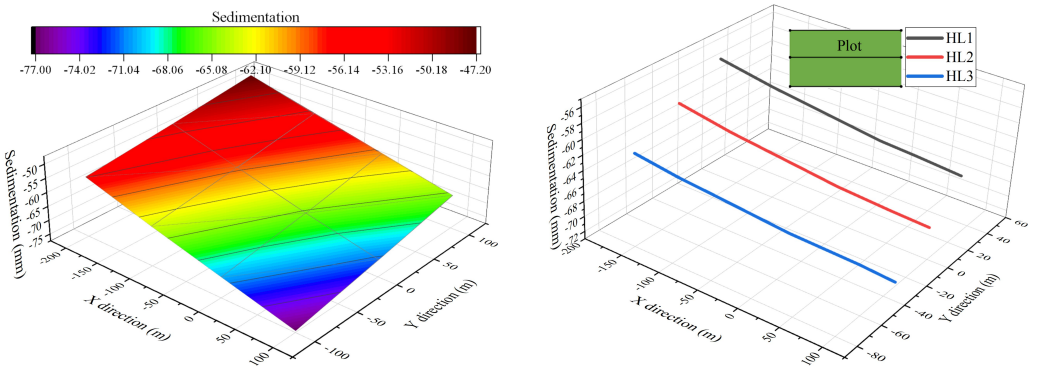

(a) Subsidence contour map

(b) Boundary subsidence line

Fig. 19 Three-dimensional subsidence contour map and boundary subsidence line of the plot 50 years later

a mixture of brine, backfill alkali slag, and sediment materials. As brine pressure rises and gradually dissipates, the surface subsidence of the mining area slows down.

(3) Stop stage. In this stage, some mining wells have entered the "hardening" phase of backfill alkali slag and sediment materials. Brine has mostly been expelled from the cavern, and the backfill alkali slag and sediment materials continue to be compressed, significantly increasing their inhibitive effect. The settlement of the mining area almost halts.

4.4 Stability evaluation of a target area

The surface of the mining area is covered by several buildings. To evaluate the stability of a small area within the mining zone, a rectangular plot as shown in Fig. 16 was selected for stability analysis. This selected plot is located near the salt mining wells W9-W10. In order to accurately calculate the tilt and uneven subsidence of the plot over the next 50 years, five vertical lines were drawn along the long side of the plot (northeast direction) and three horizontal lines were drawn along the short side (northwest direction), all with equal spacing. This setup results in 15 analysis points.

Fig. 17 shows the cumulative subsidence curves of four corner points (p1, p3, p4, and p6) of the target plot over the next 50 years. The subsidence trend of the corner points of the plot is consistent with the BR1. The predication results indicate that within the next 40 to 50 years, the target plot will reach a

state of equilibrium. The maximum subsidence at corner points p3 and p4 will be 71.38 mm; point p6 will experience 63.44 mm of subsidence; and point p1 will have the smallest subsidence of 51.86 mm. The maximum subsidence of the plot over the next 50 years is 71.38 mm, which is significantly smaller than the 200 mm specified in China's Code for Design of Building Foundation (GB50007-2011) (China, 2011). Therefore, the subsidence control of the plot meets the regulatory requirements.

The target plot is located at the edge of the subsidence slope on the mine surface, with an overall inclination towards the southeast corner, as shown in Fig. 18. The subsidence difference on both sides of the upper boundary HL1 is 12.20 mm, resulting in a tilt rate of 0.050‰; the subsidence difference on both sides of the middle boundary HL2 is 12.75 mm, resulting in a tilt rate of 0.052‰; the subsidence difference on both sides of the lower boundary HL3 is 12.94 mm, resulting in a tilt rate of 0.053‰; the subsidence difference between the northwest and southeast corners is 17.52 mm, resulting in a tilt rate of 0.069‰ (Fig. 19).

According to Article 5.3.4 of the Code for Design of Building Foundation (GB50007-2011) (China, 2011): when the height of a building exceeds 100 meters, the overall tilt rate should not exceed 2‰; when the building height is between 60 and 100 meters, the overall tilt rate should not be greater than 2.5‰.

The maximum tilt rate of the northwest and southeast corners (diagonal) of the target plot is the largest, which is 0.069‰. This indicates that the maximum tilt rate over the next 50 years will be much smaller than the limits set by the Code for Design of Building Foundation (GB50007-2011), and the tilt rate control for the plot also meets the regulatory requirements.

5 Conclusions

Based on rock mechanics and creep test parameters, combined with the subsidence monitoring data of the bedrock marker, a subsidence inversion study was conducted for the mining area. The theoretical model was continuously improved based on the inversion results, ultimately determining the fundamental parameters and calculation methods suitable for deformation inversion of mining area. This approach successfully reproduced the subsidence trend of the bedrock marker and surrounding buildings over the past eight years, with a maximum deviation of 14.82%, validating the effectiveness of the model.

The subsidence inversion and prediction results indicate that the studied mining area exhibits a large-scale, slow, uniform, and gradually converging subsidence pattern over time. The subsidence center is expected to gradually shift towards the southeast. The path of movement of the subsidence center is primarily influenced by the closure time of each mining well and the degree of consolidation of the backfill alkali slag.

The subsidence rate of the selected plot gradually decreases over the next 50 years and ultimately converges to a stable state. The maximum cumulative subsidence and tilt rate are approximately 71.38 mm and 0.069‰, respectively, both of which comply with the requirements of standards in China. The orderly mining operation and backfilling of alkali slag can ensure the long-term stability of the mining area and the safety of surrounding buildings..

Acknowledgements

The authors would like to acknowledge the financial supports from the National Natural Science Foundation of China (Grant No. 52208342), the Jiangxi Provincial Natural Science Foundation (Grant Nos. 20242BAB23037, 20232BAB204072), the Jiangxi Association for Science and Technology Foundation (Grant No. 2025QT11) and Young Elite Scientists Sponsorship Program by CAST (Grant No. 2022QNRC001). The authors would like to thank the anonymous reviewers and Editors for their constructive suggestions which greatly improve the quality of the manuscript. Thanks to the Huai'an Municipal Bureau of Natural Resources and Planning, the Huai'an District Housing and Urban-Rural Development Bureau, and Jiangsu Suyan Jingshen Co., Ltd. for their support in data research and material collection for this study.

Conflict of interest

The authors declare no competing interest.

References

Babaryka A, Benndorf J. 2023. Ground Subsidence above Salt Caverns for Energy Storage: A Comparison of Prediction Methods with Emphasis on Convergence and Asymmetry. *Mining*, **3**(2):334–346. doi:10.3390/mining3020020.

Bai WZ, Shi XL, Yang CH, et al. 2024. Assessment of the potential of salt mines for renewable energy peaking in China. *Energy*, **300**:131577. doi:10.1016/j.energy.2024.131577.

Belgian-Standards. 1998. Gas Supply Systems - Underground Gas Storage - Part 1: Functional Recommendations For Storage In Aquifers. In.

Bell F, Stacey T, Genske D. 2000. Mining subsidence and its effect on the environment: some differing examples. *Environmental Geology*, **40**:135–152. doi:10.1007/s002540000140.

Bérest P. 2017. Cases, causes and classifications of craters above salt caverns. *International Journal of Rock Mechanics and Mining Sciences*, **100**:318–329. doi:10.1016/j.ijrmms.2017.10.025.

Chen F, Ye LL, Ma HL, et al. 2022. Subsidence above gas storage in salt caverns predicted with viscoelastic theory. *Journal of Natural Gas Science and Engineering*, **103**:104620. doi:10.1016/j.jngse.2022.104620.

Chen XS, Li YP, Tong LH, et al. 2023. Elastoplastic Damage Behavior of Rocks: A Case Study of Sandstone and Salt Rock. *Rock Mechanics and Rock Engineering*, **56**(8):5621–5634. doi:10.1007/s00603-023-03349-5.

Chen XS, Xiong TK, Li YP. 2024. Research on the helium seepage mechanism in the strata surrounding bedded salt cavern helium storage and its tightness evaluation. *Geoenergy Science and Engineering*, **238**:212870. doi:10.1016/j.geoen.2024.212870.

China, Ministry of Housing and Urban-Rural Development. 2011. *Code for Design of Building Foundation*. China Architecture & Building Press.

Daupley X, Fabriol R, Contrucci I, et al. 2010. Multiparameter monitoring of a salt cavern collapse (Cerville-Buissoncourt site, France). EGU General Assembly Conference Abstracts.

Evans D, Parkes D, Dooner M, et al. 2021. Salt cavern exergy storage capacity potential of UK massively bedded halites, using compressed air energy storage (CAES). *Applied Sciences*, **11**(11):4728. doi:10.3390/app11114728.

Gwiazda P, Klawe FZ, Owczarek S. 2015. Thermo-visco-elasticity for Norton–Hoff-type models with homogeneous thermal expansion. *Nonlinear Analysis: Real World Applications*, **26**:199–228. doi:10.1016/j.nonrwa.2015.05.009.

Hashash Y, Whittle A. 1992. Integration of the modified Cam-Clay model in non-linear finite element analysis. *Computers and geotechnics*, **14**(2):59–83. doi:10.1016/0266-352X(92)90015-L.

Ji GD, Yang CH, Xu YL, et al. 2014. Laboratory test study of sedimentation and consolidation behaviors of alkali waste backfill in salt caverns. *Rock Soil Mech*, **35**(2):407–412.

Langer M. 1993. Use of solution-mined caverns in salt for oil and gas storage and toxic waste disposal in Germany. *Engineering Geology*, **35**(3-4):183–190. doi:10.1016/0013-7952(93)90005-W.

Li P, Li YP, Shi XL, et al. 2023. Experimental and theoretical research on the debrining process in sediments for a gas storage salt cavern. *Geoenergy Science and Engineering*, **225**:211667. doi:10.1016/j.geoen.2023.211667.

Li P, Li YP, Shi XL, et al. 2022. Compaction and restraining effects of insoluble sediments in underground energy storage salt caverns. *Energy*, **249**:123752. doi:10.1016/j.energy.2022.123752.

Li X, Wang SJ, Liu TY, et al. 2004. Engineering geology, ground surface movement and fissures induced by underground mining in the Jinchuan Nickel Mine. *Engineering Geology*, **76**(1-2):93–107. doi:10.1016/j.enggeo.2004.06.008.

Liu W, Li QH, Yang CH, et al. 2023. The role of underground salt caverns for large-scale energy storage: A review and prospects. *Energy Storage Materials*, 103045. doi:10.1016/j.ensm.2023.103045.

Liu W, Zhang X, Fan JY, et al. 2020. Study on the mechanical properties of man-made salt rock samples with impurities. *Journal of Natural Gas Science and Engineering*, **84**:103683. doi:10.1016/j.jngse.2020.103683.

Lyu C, Kong XXY, Zeng ZQ. 2024. A new model for predicting surface subsidence of twin salt cavern gas storages with different shapes. *Environmental Earth Sciences*, **83**(22). doi:10.1007/s12665-024-11922-6.

Minkley W, Brandt M, Dostal V, et al. 2022. Energy storage in salt caverns with supercritical CO_2. In *The Mechanical Behavior of Salt X* (pp. 639–651). CRC Press.

National-Energy-Administration-of-China. 2011. Safety rules of salt cavern underground gas storage. In. Beijing: Petroleum Industry Press.

Scigata R, Szafulera K. 2020. Linear discontinuous deformations created on the surface as an effect of underground mining and local geological conditions-case study. *Bulletin of Engineering Geology and the Environment*, **79**(4):2059–2068. doi:https://doi.org/10.1007/s10064-019-01681-1.

Shi XL, Li YP, Yang CH, et al. 2015. Influences of filling abandoned salt caverns with alkali wastes on surface subsidence. *Environmental earth sciences*, **73**:6939–6950. doi:10.1007/s12665-015-4135-y.

Tarkowski R, Uliasz-Misiak B. 2022. Towards underground hydrogen storage: A review of barriers. *Renewable and Sustainable Energy Reviews*, **162**:112451. doi:10.1016/j.rser.2022.112451.

Wan JF, Meng T, Li JL, et al. 2023. Energy storage salt cavern construction and evaluation technology. *Advances in Geo-Energy Research*, **9**(3). doi:10.46690/ager.2023.09.01.

Warren JK. 2006. *Evaporites: sediments, resources and hydrocarbons*. Springer Science & Business Media.

Warren JK. 2016. Solution mining and salt cavern usage. *Evaporites: a geological compendium*, 1303–1374. doi:10.1007/978-3-319-13512-0-13.

Xu CJ, Ding HB, Tong LH, et al. 2019. Scattering of a plane wave by shallow buried cylindrical lining in a poroelastic half-space. *Applied mathematical modelling*, **70**:171–189. doi:10.1016/j.apm.2019.01.029.

Xu YL, Yang CH, Chen F, et al. 2014. Experimental study on one-dimensional settlement of alkali wastes backfilled to abandoned salt caverns. *Chinese Journal of Geotechnical Engineering*, **36**(3):589–596. doi:10.11779/CJGE201403025.

Xu Y. 2014. *A Study of long term mechanical hehavior of salt caverns filled with mixtres of alkali wastes and brine*. University of Chinese Academy of Sciences]. Wuhan, China.

Xu YL, Yang CH, Li YP, et al. 2012. Preliminary study of the interaction between backfill body and surrounding rock salt mass. *Mechanical behaviour of salt VII*. CRC Press, Boca Raton.

Yang CH, Jing WJ, Daemen JJK, et al. 2013. Analysis of major risks associated with hydrocarbon storage caverns in bedded salt rock. *Reliability Engineering & System Safety*, **113**:94–111.

Yang CH, Wang TT, Chen H. 2023. Theoretical and technological challenges of deep underground energy storage in China. *Engineering*, **25**:168–181. doi:10.1016/j.eng.2022.06.021.

Yang J, Liu ZY, Yang CH, et al. 2021. Mechanical and microstructural properties of alkali wastes as filling materials for abandoned salt caverns. *Waste and Biomass Valorization*, **12**:1581–1590. doi:10.1007/s12649-020-01104-3.

Yao YF, Yang CH, Li YP, et al. 2011. The layout parameters of well groups and effect on land subsidence for salt mine in Zhangshu tourist area. *Procedia Engineering*, **26**:1682–1691. doi:10.1016/j.proeng.2011.11.2354.

Ye LL, Chen F, Ma HL, et al. 2022. Subsidence above rock salt caverns predicted with elastic plate theory. *Environmental Earth Sciences*, **81**(4):123. doi:10.1007/s12665-022-10232-z.

Zhang GM, Wang LJ, Wu Y, et al. 2017. Failure mechanism of bedded salt formations surrounding salt caverns for underground gas storage. *Bulletin of Engineering Geology and the Environment*, **76**:1609–1625.

Zhang GM, Wang ZS, Wang LJ, et al. 2019. Mechanism of collapse sinkholes induced by solution mining of salt formations and measures for prediction and prevention. *Bulletin of Engineering Geology and the Environment*, **78**:1401–1415. doi:10.1007/s10064-017-1173-6.

Zhang GM, Wang ZS, Zhang K, et al. 2018. Collapse mechanism of the overlying strata above a salt cavern by solution mining with double-well convection. *Environmental Earth Sciences*, **77**:1–16. doi:10.1007/s12665-018-7739-1.

Zhang N, Liu XC, Zhang Y, et al. 2024. Investigating the Mechanism of Land Subsidence Due to Water Network Integration at the Guangzhou Longgui Salt Mine and Its Impact on Adjacent Subway. *Water*, **16**(12):1723–1739. doi:10.3390/w16121723.

Zhang N, Yang J, Shi XL, et al. 2020. Ground subsidence mechanism analysis of Longgui salt rock mining area: Case study. *Thermal Science*, **24**(6 Part B):3869–3875. doi:10.2298/TSCI2006869Z.